Organic Geochemistry 208 (2025) 105049

Contents lists available at ScienceDirect

Organic Geochemistry

journal homepage: www.elsevier.com/locate/orggeochem

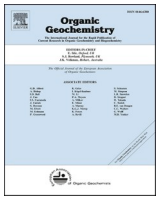

Geochemical implications of the carbon isotope compositions of individual polycyclic aromatic compounds in coals from the Junggar and Ordos basins, NW China

Ziao Geng [a,b,c], Meijun Li [a,b,c,*], Shuichang Zhang [d], Shengbao Shi [c], Wenqiang Wang [e,f], Lei Zhu [c], Tiantian Li [c], Jianfeng Zhang [a,b,c]

[a] Hainan Institute of China University of Petroleum (Beijing), Sanya, Hainan 572025, China
[b] National Key Laboratory of Petroleum Resources and Engineering, Beijing 102249, China
[c] College of Geosciences, China University of Petroleum (Beijing), Beijing 102249, China
[d] Research Institute of Petroleum Exploration and Development, PetroChina, Beijing 100083, China
[e] School of Earth Sciences and Engineering, Xi'an Shiyou University, Xi'an, Shaanxi 710065, China
[f] Shaanxi Key Laboratory of Petroleum Accumulation Geology, Xi'an Shiyou University, Shaanxi 710065, China

ARTICLE INFO

Associate Editor – Prasanta Sanyal

Keywords:
Coals
Northwestern China
PACs
Carbon isotope composition
Wildfires
Isotopic fractionation

ABSTRACT

This study analyzes the $\delta^{13}C$ values of various polycyclic aromatic compounds (PACs), including dibenzofuran, and methyldibenzofurans in two sets of coals from the Junggar and Ordos basins in NW China. The results reveal that the $\delta^{13}C$ values of individual PACs are primarily influenced by the source of degraded organic matter rather than thermal maturity. The significant differences in $\delta^{13}C$ values (−11.7 ‰) between dibenzofuran (DBF) and its methylated homologues (MDBFs) imply different sources. DBF is primarily derived from higher plants, while MDBFs have multiple sources from both lichens and higher plants. However, the $\delta^{13}C$ values of DBF and MDBF in predominantly pyrogenic samples are relatively similar. This is due to two factors: (1) The kinetic isotope effect leads to preferential demethylation of ^{12}C-enriched MDBF isomers, and the residual MDBFs are consequently enriched in ^{13}C isotopes. The DBF produced by this process is enriched in ^{12}C isotope, leading to depletion of $\delta^{13}C$ for DBF in the combustion products. (2) Greater higher plant than lichen inputs result in higher $\delta^{13}C$ values of MDBFs also potentially causes lower $\delta^{13}C$ values in DBF. These two factors combine to produce similar $\delta^{13}C$ values for DBF and MDBFs in samples heavily affected by wildfires.

1. Introduction

Aromatic compounds—including fluorene (Flu), dibenzofuran (DBF), dibenzothiophene (DBT), naphthalene (N), phenanthrene (Phen), and their alkyl isomers—are commonly found in sedimentary and petroleum organic matter (OM). Variations in the molecular distributions of these compounds have been given considerable attention in the field of organic geochemistry as they can serve as indicators of the thermal histories, sources, and environmental conditions of sediments (Radke et al., 1982, 2000; Hughes et al., 1995; Santamaria-Orozco et al., 1998; Widodo et al., 2009; Li et al., 2013a). The distributions of aromatic compounds vary considerably among sediments and oil samples since they are influenced by thermal maturity, source, biodegradation and weathering (Budzinski et al., 1995; van Aarssen et al., 1999; Asif et al., 2009; Marynowski et al., 2011).

Aromatic compounds are primarily formed by geosynthetic processes, which produce a range of isomerized, alkylated, and dealkylated components. Previous research has focused on the molecular distributions of aromatic compounds and their significance for understanding thermal evolution and diagenesis of natural precursors (Radke et al., 1986; Alexander et al., 1995; Asif et al., 2009, 2010; Li et al., 2013b; Zhu et al., 2019, 2022) and for tracing oil filling pathways (Wang et al., 2020). However, some studies have suggested that a proportion of the aromatic compounds originates from combustion, and these have been increasingly used as indicators of burning vegetation in sedimentary records (van Aarssen et al., 1999; Watson et al., 2005; Jiang and George, 2019, 2020; Karp et al., 2020; Zakrzewski and Kosakowski, 2021; Li et al., 2022). Compounds such as cadalene (Cad), retene (Ret),

* Corresponding author at: National Key Laboratory of Petroleum Resources and Engineering, Beijing 102249, China.
E-mail address: meijunli2008@hotmail.com (M. Li).

https://doi.org/10.1016/j.orggeochem.2025.105049
Received 8 December 2024; Received in revised form 11 June 2025; Accepted 7 July 2025
Available online 23 July 2025

Table 1
Geochemical characteristics of the coals from outcrops in the Ordos basin and Junggar basin.

Basin	Sampling site	Sample name	Formation	%R_o	T_{max}	TOC (%)
Ordos basin	Puxian	PX-S22	C-P	0.62	435	83.1
		PX-S6	C-P	0.63	444	84.3
	Baode	BD-S24	C-P	0.62	444	68.6
		BD-S21	C-P	0.63		
	Xingxian	XX-S10	C-P	0.73	440	74.3
	Linxian	LX-S8	C-P	1.03	455	71.2
		LX-S11	C-P	0.77	444	77.9
		LX-S20	C-P	1.08	462	79.2
	Liulin	LL-S5	C-P	1.27	489	75.1
		LL-S25	C-P	1.40	493	84.3
	Yaping	YP-S9	C-P	1.36	484	82.4
	Hancheng	HC-S4	C-P	1.88	501	83.8
Junggar basin	Liuhuanggou	LHG-A6	J_2x	0.47	427	70.2
		LHG-E3	J_2x	0.52	431	71.4
		LHG-A10	J_2x	0.46	434	63.4
		LHG-E5	J_2x	0.46	426	71.5
	Tiechanggou	TCG-A9	J_2x	0.49	441	67.0
		TCG-F7	J_2x	0.76	449	84.4
		TCG-F9	J_2x	0.46	444	81.7
	Jimusaer	JMSR-A3	J_2x	0.46	428	79.6
		JMSR-B11	J_2x	0.52	429	80.5
		JMSR-S17	J_2x	0.53	432	46.0
	Changji	CJ-F5	J_1b	0.60	430	73.7
	Dahuangshan	DHS-F10	J_1b	0.53	431	77.6
		DHS-B7	J_1b	0.82	426	77.8
	Hutubi	HTB-A4	J_1b	0.75	447	84.3
		HTB-A8	J_1b	0.68	444	82.0
		HTB-A7	J_1b	1.08	454	86.3
	Houxia	HX-D1	J_1b	0.60	436	81.3

%R_o: vitrinite reflectance; T_{max}: temperature at maximum generation; TOC = total organic carbon; C-P = Carboniferous-Permian; J_1b = Lower Jurassic Badaowan Formation; J_2x = Middle Jurassic Xishanyao Formation.

simonellite (Sim), and 6-isopropyl-1-isohexyl-2-methylnaphthalene (ip-iHMN) were identified as indicators of terrestrial plants (Ellis et al., 1996; Lei et al., 2022; Martins et al., 2020; van Aarssen et al., 1992, 2000), and the higher plants index (HPI) has also been proposed as a means of determining the relative input from vascular plants (van Aarssen et al., 2000), provide useful information for understanding source inputs.

The primary carbon isotope composition ($\delta^{13}C$) of sedimentary organic matter is influenced by water column carbon cycling, environmental conditions during formation, fractionation during photosynthesis, and efficiency of dissolved inorganic carbon uptake (Galimov, 2006). This information provides valuable insights into the source and biosynthesis of sedimentary organic matter (Boreham et al., 1994; Radke et al., 1998; Sephton et al., 2000). In recent years, analysis of the $\delta^{13}C$ of individual compounds using compound-specific isotope analysis (CSIA) has emerged as an effective tool for assessing the molecular-level sources and diagenetic pathways of compounds and has been successfully applied to identify the origins of saturated compounds such as *n*-alkanes and cadinanes (Boreham et al., 1994; Murray et al., 1998). However, due to interference between compounds in a complex mixture, it is difficult to precisely determine the carbon isotopic composition of individual PACs. Some recent research has established the process for the separation of PACs (Konan et al., 2022). In such cases, the $\delta^{13}C$ values of individual aromatic compounds are crucial for determining the origins of organic matter (Maslen et al., 2011; Cesar and Grice, 2017; Karp et al., 2020; Niu et al., 2023). Although some studies have indicated that the isotopic compositions of individual aromatic compounds are affected by the thermal maturity of their organic materials (Le Métayer et al., 2014; Chen et al., 2016), more recent research has demonstrated that the isotopic compositions of individual compounds are primarily dictated by the source of the parent material, with less impact from secondary processes such as thermal maturity and biodegradation (Boreham et al., 1994; Radke et al., 1998; Mazeas et al., 2002).

Wildfires have a significant impact on terrestrial ecosystems, it may threaten the stability of forests and leading to a sharp decline in biodiversity (Hua et al., 2024) and are also suggested as ecological and evolutionary force in shaping structure and function of forest ecosystem (He and Lamont, 2018). The PACs that derive from combustion can provide additional insights into the type of plant communities that were destroyed by fire. Previous research has indicated that certain alkylated PAH structures and the $\delta^{13}C$ of individual aromatics can be used to differentiate between plant types (Widodo et al., 2009; Cesar and Grice, 2017; Karp et al., 2020). Parameters such as dimethylphenanthrene (DMP) ratios have been used as indicators for changes in burned plant communities (Karp et al., 2020; Zakrzewski and Kosakowski, 2021). The sources of PAHs can be determined by interpretation of the relative abundance of alkyl PAHs, where the predominance of C_1 (alkylated PAHs) indicates the petrogenic origin PAHs. The predominance of C_0 (non-alkylated) PAHs are usually associated with the pyrolytic source PAHs (Yunker et al., 2002; Kappenberg et al., 2019; Zakrzewski and Kosakowski, 2021). However, the $\delta^{13}C$ systematics of individual aromatic compounds derived from plants and wildfires are largely unknown, including their preservation in geological records.

The aim of this paper is to examine the factors impacting the $\delta^{13}C$ values of the individual PACs including DBF, and MDBFs, and provide

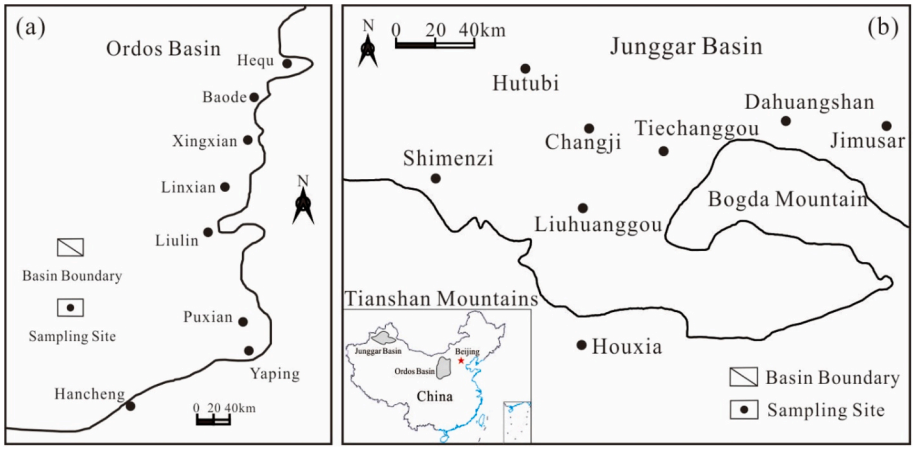

Fig. 1. Sketch maps showing the location of coals in the Ordos and Junggar Basins, Western China (modified after Zhu et al., 2019).

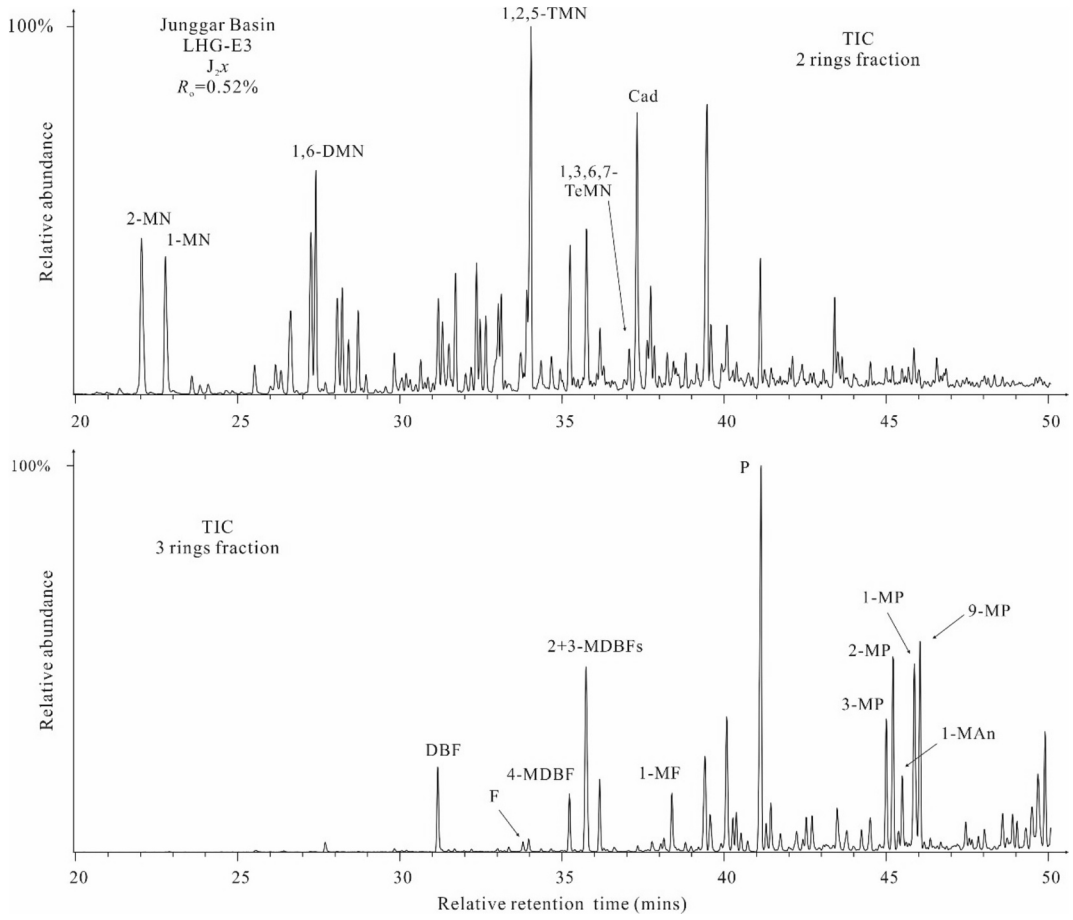

Fig. 2. Total ion chromatograms of the 2 rings and 3 rings fractions separated from the LHG-E3 sample, showing the distribution of 2-ring and 3-ring aromatic hydrocarbons.

insights to their general use. Considering the previous research on wildfires of the Junggar and Ordos basins during the Jurassic and C-P, the coals from these two basins are useful as cases for the discussion of the impact of wildfires on $\delta^{13}C$ of individual PACs.

2. Samples and geological setting

A total of 29 coal samples were collected from the Ordos and Junggar basins in China (Table 1). The Ordos Basin is an intracratonic depression basin located in north-western China (Fig. 1a), which is characterized by 250×10^3 km^2 of the Paleozoic strata (Zhu et al., 2019, 2022). The widely distributed Carboniferous-Permian coals and coal-measure mudstones deposited in a marine-terrestrial transitional sedimentary environment and covering an area of 180×10^3 km^2, which are the primary source rocks for the Upper Paleozoic gas fields in this basin (Dai et al., 2005; Qi et al., 2020; Niu et al., 2024; Han et al., 2024). During the Early Cretaceous, incursion of hydrothermal fluids in the southeastern part of the Ordos basin caused alteration of the Upper Paleozoic strata (Yang et al., 2005; Qin et al., 2017). In the Ordos basin, 12 coal samples were collected from Carboniferous-Permian coal seams. These coals have total organic carbon (TOC) values ranging from 68.6 % to 84.3 %. Coals from the Ordos basin have relatively high thermal maturity, with vitrinite reflectance (R_o) values ranging from 0.62 % to 1.88 % (average 1.0 %), and T_{max} values ranging from 435 to 501 °C (average 463 °C) (% $R_o \geq 0.5$, T_{max} >435 °C indicate mature).

The Junggar Basin is a significant coal-bearing continental superimposed basin which located in the northern part of the Xinjiang Uygur Autonomous Region of China (Fig. 1b) and covers an area of 1.3×10^5 km^2 (Zhu et al., 2019; Wu et al., 2020). The basin is characterized by the 3000 m-thick strata of coal accumulation, which including the Lower Jurassic Badaowan Formation (J_1b), the Sangonghe Formation (J_1s), and the Middle Jurassic Xishanyao Formation (J_2x) (Li et al., 2012; Qian et al., 2018; Ge et al., 2024). The J_1b consists of fluvial and paludal sediments. A transgressive event occurred during the J_2x period leading to the development of alternating lacustrine shore, fluvial, and deltaic facies (Li et al., 2018; Tang et al., 2021). Research on the origins of organic parent material and sedimentary environments suggests that during the deposition period of J_1b, land plants were not abundant in the Junggar area, while higher plants thrived during the J_2x deposition period, which coincided with a warm global palaeoclimate with high concentrations of atmospheric oxygen (Li et al., 2018; Xie et al., 2022), which created favorable conditions for wildfire events. A suite of 17 coal samples were collected from the Badaowan (J_1b) and Xishanyao (J_2x) formations in the Junggar Basin. The J_1b samples were further divided into J_1b I and J_1b II based on differences in geochemical characteristics (Pr/Ph, Pr/nC$_{17}$ versus Ph/nC$_{18}$, C$_{27}$/C$_{29}$, and C$_{27}$, C$_{28}$, and C$_{29}$-steranes), which will be discussed in detail later. These coals have TOC contents ranging from 46.0 % to 86.3 % (Table 1). Unlike the coals from the Ordos Basin, most of the coals from the Junggar Basin are immature-to-mature, with vitrinite reflectance (R_o) values ranging from 0.46 % to 1.08 % (average 0.60 %) and T_{max} values ranging from 426 to 454 °C (average 436 °C). The wide ranges of thermal maturity and OM sources covered by the samples from these two basins can provide a broad comparison for $\delta^{13}C$ systematic study.

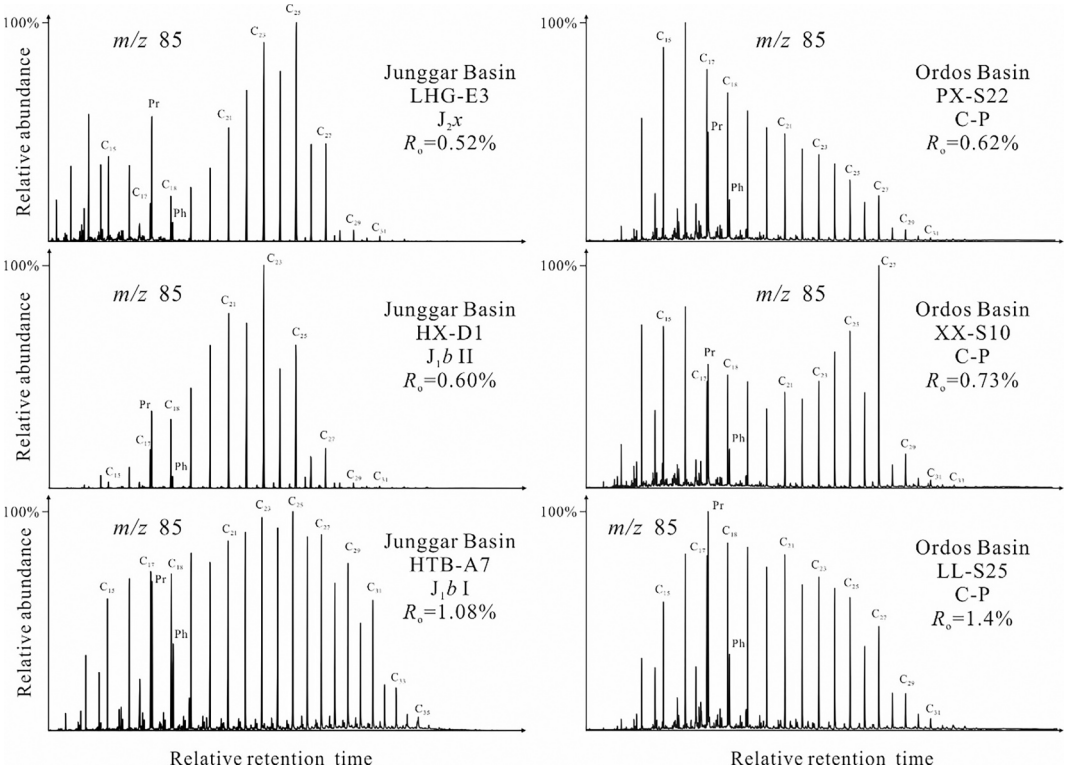

Fig. 3. *n*-Alkane distributions (*m/z* 85 partial mass chromatograms) of saturated hydrocarbon fractions in six representative samples.

3. Materials and methods

3.1. TOC, Rock-Eval, and vitrinite reflectance measurements

The coal samples were analysed using the method described in Zhu et al., 2019. Prior to TOC analysis, all coals were treated with HCl and deionized water to remove carbonates and contaminants. After pretreatment with HCl and deionized water, TOC was analyzed using a LECO CS-230 carbon/sulfur apparatus. Rock-Eval pyrolysis was performed on powdered coal samples (15 mg) using an OGE-VI Rock Pyrolysis analyzer. The vitrinite reflectances (%R_o) of polished coal blocks were determined using a Leica Model MPV-SP microscopic photometer according to the method described in Kilby (1988).

3.2. Coal extraction and GC–MS analysis

The analytical procedures used are described in Zhu et al., 2022. The coal samples were crushed, ground to <80 mesh (0.2 mm), and processed for 48 h using a Soxhlet apparatus with 400 mL of dichloromethane to extract soluble organic matter. The coal extracts were treated using petroleum ether to remove asphaltenes. The solutions were then separated into saturated, aromatic, and resin fractions using a silica gel/alumina chromatography column with petroleum ether, dichloromethane/petroleum ether (2:1, v/v), and dichloromethane/methanol (93:7, v/v), respectively, as the elution solvents.

GC–MS analyses of the saturated and aromatic fractions and comparisons with authentic standards were conducted using an Agilent 6890 gas chromatograph coupled to an Agilent 5975i mass spectrometer equipped with an HP-5MS fused silica capillary column (60 m × 0.25 mm i.d., 0.25 μm film thickness). The GC–MS analyses of the saturated fractions were conducted under the following conditions: the initial GC oven temperature was maintained at 50 °C for 1 min, then ramped to 120 °C at a rate of 20 °C/min, then increased from 120 °C to 310 °C at 3 °C/min, and finally held constant for 25 min. For the aromatic fractions and the authentic standards, the initial temperature of the GC oven was set at 80 °C, maintained for 1 min, then gradually increased to 310 °C at 3 °C/min, and finally held constant for 16 min. Helium was used as the carrier gas and the temperature of the split/splitless injector was set at 300 °C. The MS was operated with the electron ionization (EI) source set at 70 eV and a scan range of *m/z* 50–600. Peak areas of each compound were integrated using the Agilent ChemStation Data Analysis software, the relative concentration, indices and molecular ratios in this study are based on the data from this result.

3.3. Sub-separation of aromatic compounds

Ten samples of different thermal maturity and depositional environment from two basins were selected for sub-separation and isotopic analysis. The aromatic compounds obtained from the previous separation were separated into mono-, di-, tri- and larger (tetracyclic and higher) aromatic compounds. The silica gel and cotton wool were Soxhlet extracted by dichloromethane for 72 h. A small amount of pre-extracted cotton wool was placed at the bottom of a glass column (20 cm in length and 10 mm inner diameter), preventing leakage of the stationary phase. Alumina (obtained from the Sigma company) was activated at 110 °C for 4 h, and the pre-extracted silica was also activated at 110 °C for 4 h. Then, 2–3 g of the activated alumina and an equal volume of silica (silica on the bottom, alumina on the top) were inserted into the glass column, and the column was knocked to ensure even distribution of the alumina. Next, the aromatic compounds were transferred into the column. The column was eluted using petroleum ether:dichloromethane (93:7 v:v, 6 mL), petroleum ether:dichloromethane (9:1 v:v, 8 mL), petroleum ether:dichloromethane (3:1 v:v, 8 mL) and dichloromethane (8 mL), respectively, for the mono-, di- (2 rings), tri- (3 rings), and larger aromatic fractions. The 2 rings to 3 rings fractions of the representative sample are shown in Fig. 2. The selected PAHs (DBF and MDBFs) show sufficient baseline resolution and minimal co-elution such that we can measure their individual stable carbon isotopic values.

Table 2
Results of biomarker indicators referred to in the text.

Basin	Sample Name	Formation	*n*-Alkane and isoprenoid ratios				Regular sterane and ratios				1,7-DMP/(1,7-+2,6 + 3,5-DMP)	Fl/(Fl + Py)	BaA/(BaA + Chr)	$C_0/(C_0 + C_1)$ Fl/Py	IPy/(IPy + BgP)
			Pr/Ph	Pr/C_{17}	Ph/C_{18}	CPI	C_{27}%	C_{28}%	C_{29}%	C_{27}/C_{29}					
Ordos basin	PX-S22	C-P	2.30	0.95	0.45	1.41	26.15	17.62	56.23	0.46	0.63	0.54	0.49	0.53	0.25
	BD-S24	C-P	3.28	2.46	0.74	1.23	23.35	24.71	51.94	0.45	0.62	0.56	0.51	0.54	0.41
	XX-S10	C-P	2.80	1.70	0.56	2.29	29.30	19.96	50.74	0.58	0.64	0.60	0.42	0.59	0.53
	LX-S20	C-P	2.02	0.14	0.08	1.09	33.00	24.30	42.70	0.77	0.64	0.45	0.21	0.38	0.25
	LL-S25	C-P	2.70	1.90	0.63	1.45	27.91	20.43	51.66	0.54	0.63	0.55	0.50	0.54	0.35
	LX-S8	C-P	0.56	0.30	0.21	1.05	25.86	17.46	56.67	0.46	0.67	0.44	0.18	0.41	0.16
	LX-S11	C-P	1.58	0.32	0.14	1.06	30.23	21.99	47.78	0.63	0.69	0.49	0.21	0.41	0.18
	BD-S21	C-P	1.70	1.35	0.47	1.23	24.38	24.41	51.21	0.48	0.61	0.59	0.50	0.50	0.42
	LL-S5	C-P	0.51	0.55	0.46	1.82	*n.d.*	*n.d.*	*n.d.*	*n.d.*	0.31	0.33	0.09	0.46	0.15
	HC-S4	C-P	0.27	0.54	0.71	1.28	*n.d.*	*n.d.*	*n.d.*	*n.d.*	0.16	0.46	0.08	0.55	0.28
	PX-S6	C-P	1.69	1.01	0.34	1.06	40.14	15.94	43.92	0.91	0.65	0.36	0.28	0.39	0.25
	YP-S9	C-P	0.38	0.43	0.49	1.13	*n.d.*	*n.d.*	*n.d.*	*n.d.*	0.27	0.40	0.13	0.45	0.25
Junggar basin	LHG-A6	J_2x	3.90	0.97	0.22	3.15	12.72	19.42	67.86	0.19	0.82	0.55	0.62	0.65	0.72
	LHG-E3	J_2x	7.11	4.68	0.65	2.66	17.64	26.87	55.49	0.32	0.75	0.49	0.54	0.68	0.57
	LHG-A10	J_2x	8.06	9.03	0.77	3.33	13.45	23.08	63.46	0.21	0.70	0.54	0.45	0.62	0.45
	LHG-E5	J_2x	3.92	1.88	0.32	5.56	13.59	22.03	64.38	0.21	0.91	0.60	0.63	0.60	0.71
	TCG-A9	J_2x	8.68	2.03	0.17	2.01	16.77	21.14	62.09	0.27	0.89	0.68	0.35	0.66	0.39
	TCG-F7	J_2x	7.14	2.70	0.29	1.67	24.09	21.49	54.41	0.44	0.86	0.63	0.40	0.62	0.47
	TCG-F9	J_2x	8.49	2.28	0.19	2.01	16.98	19.99	63.03	0.27	0.88	0.68	0.36	0.65	0.37
	JMSR-A3	J_2x	5.44	11.65	1.41	1.77	13.43	16.40	70.17	0.19	0.87	0.49	0.48	0.52	0.35
	JMSR-B11	J_2x	6.42	3.03	0.26	1.67	15.71	18.77	65.53	0.24	0.92	0.49	0.55	0.49	0.35
	JMSR-S17	J_2x	6.55	1.98	0.18	1.75	18.17	15.96	65.87	0.28	0.91	0.59	0.56	0.54	0.58
	CJ-F5	J_1b I	2.24	1.19	0.69	1.42	58.47	15.65	25.88	2.26	0.78	0.41	0.23	0.38	*n.d.*
	DHS-B7	J_1b I	2.43	0.29	0.14	1.14	39.65	29.22	31.13	1.27	0.61	0.49	0.22	0.41	0.19
	HTB-A7	J_1b I	1.93	1.28	0.76	1.42	57.40	16.96	25.64	2.24	0.79	0.43	0.22	0.44	*n.d.*
	DHS-F10	J_1b II	5.49	11.57	1.10	1.65	18.74	15.72	65.54	0.29	0.69	0.63	0.54	0.55	0.54
	HX-D1	J_1b II	6.38	2.79	0.25	2.84	15.38	23.88	60.74	0.25	0.81	0.65	0.59	0.68	0.58
	HTB-A4	J_1b II	3.90	10.89	1.69	1.07	23.35	23.56	53.09	0.44	0.69	0.62	0.54	0.68	0.51
	HTB-A8	J_1b II	4.12	4.35	0.63	1.67	24.04	21.65	54.31	0.44	0.72	0.66	0.56	0.68	0.53

Pr: Pristane; Ph: Phytane; DMP: dimethylphenanthrene; Fl: fluoranthene; Py: pyrene; BaA: benz[*a*]anthracene; Chy: chrysene; C_0: non-methylated PACs; C_1: methylated PACs; IPy: indeno[1,2,3-*cd*]pyrene; BgP: benzo[*ghi*]perylene; $C_0/(C_0 + C_1)$ Fl/Py = (Fl + Py)/(C_0 Fl + C_1 Fl + C_0 Py + C_1 Py); *n.d.*: not detected.

3.4. Gas chromatography-isotope ratio mass spectrometry (GC-IRMS)

0.5 μL of the concentrated aromatic sub-fraction was injected into the inlet of an Agilent 7890 GC-GC5 interface Precision IRMS (Elementar Analyzer System) operating in split mode. Separation was on an AB-PONA column (50 m × 0.20 mm i.d., 0.50 μm thick, Agilent). The temperature program for detection of 2 rings fractions is 100 °C for 1 min and then increased at 15 °C/min to180 °C, increasing to 270 °C at 1.5 °C/min, ramping to 310 °C at 15 °C/min, holding at 310 °C for 15 mins. The procedure for detecting 3 rings fractions is held at 100 °C for 1 min and increasing to 200 °C at 15 °C/min and then increased at 2 °C/min to 290 °C, ramping to 310 °C at 10 °C/min, holding at 310 °C for 20 mins. The temperature of the oxidation oven is 850 °C, using helium as the carrier gas.

The accuracy of the data was routinely monitored with a set of standards of known isotopic composition before and after each sample analysis. Briefly, the stable carbon isotope data were evaluated by analysing *n*-alkanes with known $\delta^{13}C$ values from the Biogeochemical Laboratories, Indiana University. Normally, one injection of standards was performed for every five sample injections. A CO_2 reference gas standard is calibrated to the *n*-alkane mixture standard (calibrated to Vienna Peedee Belemnite, VPDB). The resulting data are presented in delta-notation relative to the international standard (VPDB). Every sample is injected at least two times, carbon isotope data of the selected polycyclic aromatic components were analyzed at an average standard deviation of 0.5 ‰. Peaks co-eluting as well as those at very low concentrations were not considered for our interpretations.

4. Results

4.1. *n*-Alkanes and pristane/phytane

The distribution of *n*-alkanes in the *m/z* 85 partial mass chromatograms ranges between nC_{12} and nC_{36} (Fig. 3). There are differences in the *n*-alkane distribution patterns between the Ordos basin and the J_1b/J_2x samples. Short-chain *n*-alkanes (nC_{13} to nC_{20}) predominate in the samples from the Ordos basin, with Pr/Ph ratios varying from 0.27 to 3.6 (Table 2). The J_1b and J_2x coals are dominated by intermediate-chain *n*-alkanes (nC_{23} to nC_{25}), with Pr/Ph ratios ranging from 1.9 to 6.4 for J_1b, and from 3.9 to 8.7 for the J_2x samples. The dominance of odd carbon number high molecular weight *n*-alkanes range with CPI values increases from the Ordos basin (1.05–2.29) and J_1b I (1.14–1.42) through the J_1b II (1.07–2.84) to the J_2x samples (1.67–5.56).

4.2. Steranes

The distribution patterns and relative concentrations of regular steranes can be used as source parameters that can also differentiate between depositional environments (Peters et al., 2005). Regular C_{27}, C_{28}, and C_{29} steranes were detected in all coal samples (Fig. 4). Sterane formation and composition are affected by the depositional environments and diagenetic processes. C_{27} steranes originate from the cellular membranes of vertebrates, algae and plankton. C_{28} steranes are derived from C_{28}-sterols, which are precursors synthesized in some microalgae, and C_{29} steranes are indicators of higher plant cells (Huang and

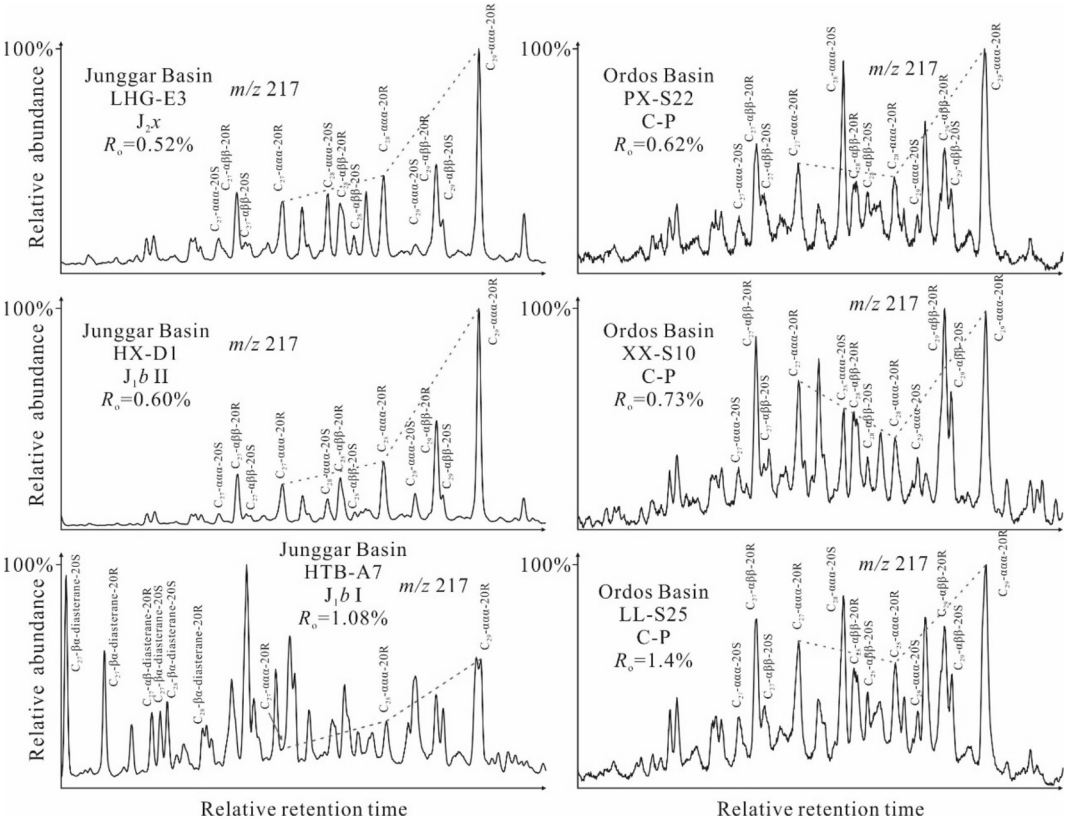

Fig. 4. Sterane and diasterane distributions (*m/z* 217 partial mass chromatograms) of the saturated hydrocarbon fractions of six representative samples.

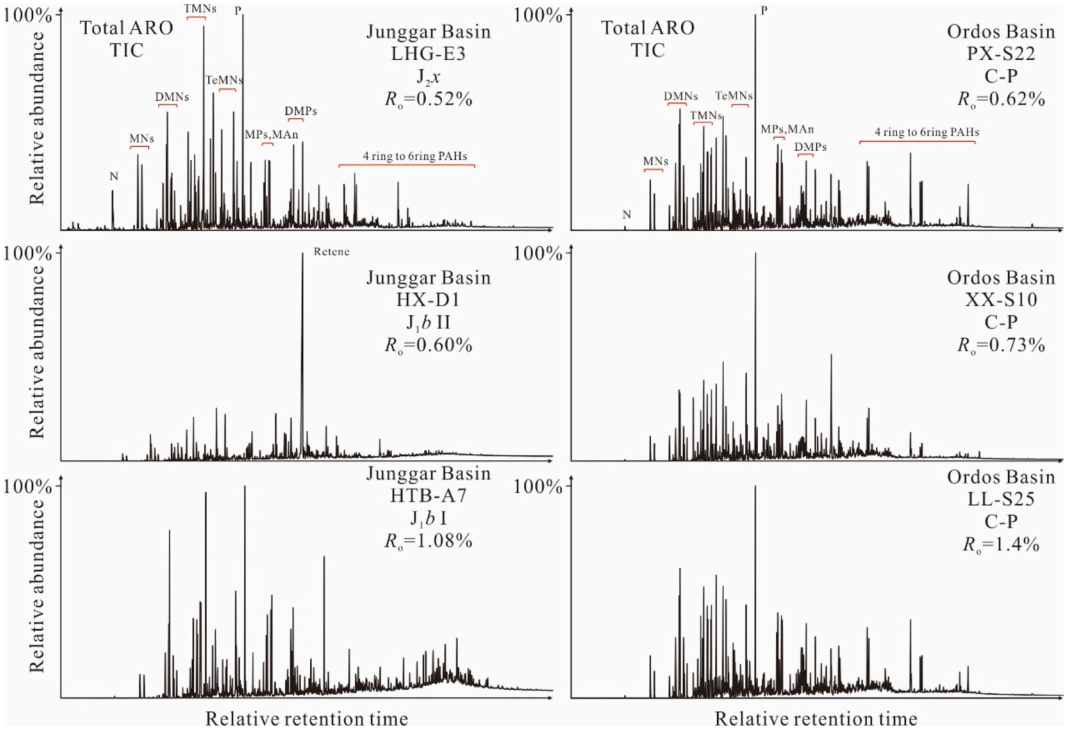

Fig. 5. Total ion chromatograms (TICs) of the aromatic compounds of six representative samples.

Meinschein, 1979; Peters et al., 2005; Volkman et al., 2005).

In this study, regular C_{27}, C_{28}, and C_{29}-steranes series were detected in all samples, with the Ordos basin and J_1b I samples all being dominated by C_{27}, C_{28}, and C_{29}-5α(H),14α(H),17α(H)-20R-cholestanes. The concentrations of C_{27} and C_{29}-steranes were significantly higher than that of C_{28} steranes, indicating similar contributions of higher plants and algae and plankton. In the samples from the Ordos basin, C_{29} regular steranes are more abundant (C_{27}/C_{29} ααα 20R steranes from 0.49 to

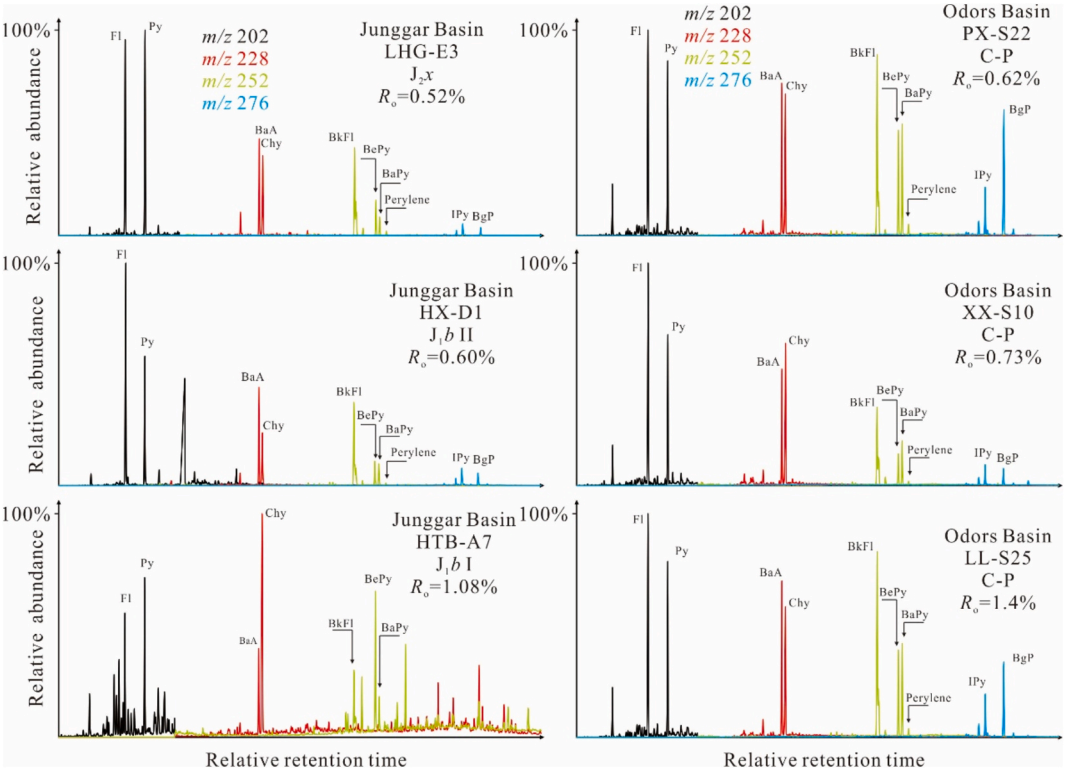

Fig. 6. Partial mass chromatograms of *m/z* 202 + 228 + 252 + 276 of the aromatic fractions of samples.

0.91), while the J_1b I samples are moderately-to-strongly dominated by C_{27} regular steranes (C_{27}/C_{29} ααα 20R steranes from 0.82 to 1.17) (Fig. 3; Table 2). The J_1b II and J_2x samples are dominated by regular C_{29}-sterane isomers (C_{27}/C_{29} ααα 20R steranes from 0.25 to 0.44) (Fig. 4).

4.3. Aromatics

Aromatic compounds have a significant role in assessing depositional environments and sources of organic matter. The distributions of aromatic compounds in the Ordos basin samples are generally similar, with a series of 2- to 6-ring PACs being identified. However, the contents of PACs in the Junggar samples are significantly different. The relative abundance of 5-ring and higher molecular weight PACs in some of the J_1b I samples are lower than those in the J_1b II and J_2x samples or are undetectable.

The total ion chromatogram of the aromatic fraction is dominated by naphthalene, alkylnaphthalenes, phenanthrene, and alkylphenanthrenes (Fig. 5). PAHs ranging from 4 to 6 rings were detected in the Ordos basin, J_2x, J_1b II, and some of the J_1b I samples (Li et al., 2012; Zakrzewski and Kosakowski, 2021), including compounds such as fluoranthene (Fl), pyrene (Py), benz[*a*]anthracene (BaA), chrysene (Chy), benzo[*k*]fluoranthene (BkFl), benzo[*e*]pyrene (BePy), benzo[*a*]pyrene (BaPy), Perylene (Pe), indeno[1,2,3-*cd*]pyrene (IPy), benzo[*ghi*]perylene (BgP) (Fig. 6).

1,7-DMP/(1,7 + 2,6 + 3.,5-DMP), Fl/(Fl + Py), BaA/(BaA + Chy), $C_0/(C_0 + C_1)$ Fl/Py, and IPy/(IPy + BgP) ratios were calculated (Table 2). The 1,7-DMP/(1,7 + 2,6 + 3.,5-DMP) ratio shows low values (0.33–0.60) in Ordos basin samples and J_1b I samples (0.41–0.49), while being higher in J_2x samples (0.49–0.68) and J_1b II samples (0.62–0.66). This applies as well to the Fl/(Fl + Py) ratio in Ordos basin and J_1b I samples (from 0.09 to 0.51, and 0.22 to 0.23), whereas in J_2x samples and J_1b II samples, the values are higher (0.35–0.63 and 0.54–0.59). The BaA/(BaA + Chy), $C_0/(C_0 + C_1)$ Fl/Py, and IPy/(IPy + BgP) ratios in Ordos basin samples (from 0.16 to 0.69, 0.38 to 0.59 and 0.15 to 0.53) are relatively dispersed. In J_2x samples, the BaA/(BaA + Chy) and IPy/(IPy + BgP) ratios reach the highest values (up to 0.92 and 0.72), while being lower and/or more consistent in J_1b I samples (0.61–0.79 and 0–0.19) and J_1b II samples (0.69–0.81 and 0.51–0.58). The $C_0/(C_0 + C_1)$ Fl/Py ratio shows relatively dispersed in J_2x samples, J_1b I samples and J_1b II samples (from 0.49 to 0.68, 0.38 to 0.44, and 0.55 to 0.68) (Table 2).

Table 3
Compound-specific carbon isotope data for dibenzofuran, and methyldibenzofurans in the coals from the Ordos basin and Junggar basin.

Basin	Sample Name	Formation	$\delta^{13}C$ (‰ vs VPDB)		
			DBF	4-MDBF	2 + 3-MDBF
Ordos basin	PX-S22	C-P	−24.1	−27.5	−29.7
	BD-S24	C-P	−28.0	−26.8	−27.7
	XX-S10	C-P	−27.4	−27.6	−26.1
	LX-S20	C-P	−24.3	−26.5	−25.1
	LL-S25	C-P	−23.5	−27.5	−29.3
Junggar basin	LHG-A6	J_2x	−25.4	−25.9	−25.5
	LHG-E3	J_2x	−26.2	−25.8	−26.8
	CJ-F5	J_1b I	−19.7	−31.6	−29.4
	DHS-B7	J_1b I	−19.8	−25.1	−26.1
	HTB-A7	J_1b I	−20.2	−30.1	−29.5

DBF: dibenzofuran; MDBF: methyldibenzofuran.

4.4. Carbon isotopic compositions of individual PACs

Ten samples from different sedimentary environments were selected for isotopic analysis of individual PACs. $\delta^{13}C$ values were measured for various PACs, including DBF, 4-MDBF, and 2 + 3-MDBFs (Table 3). In the Ordos basin samples, the $\delta^{13}C$ values of DBF range from −28.0 ‰ to −24.1 ‰; 4-MDBF are quite similar (−27.6 ‰ to −26.8 ‰); but the 2 + 3-MDBFs have a wide distribution (−29.7 ‰ to −25.1 ‰). In the

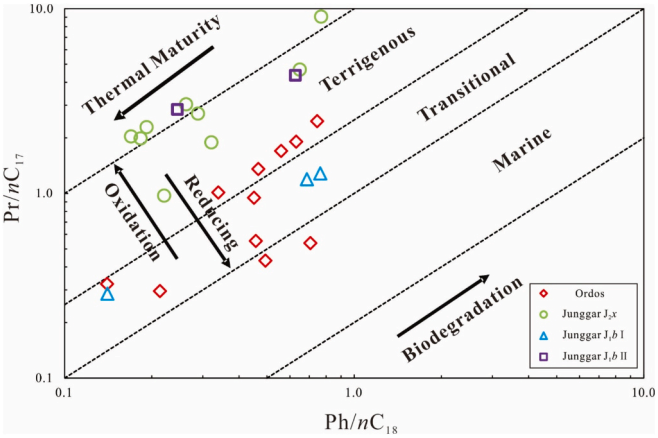

Fig. 7. Cross-plot of phytane/nC_{18} and pristane/nC_{17} for the coals from the Ordos and Junggar basins showing their depositional conditions and types of organic matter (after Shanmugam, 1985).

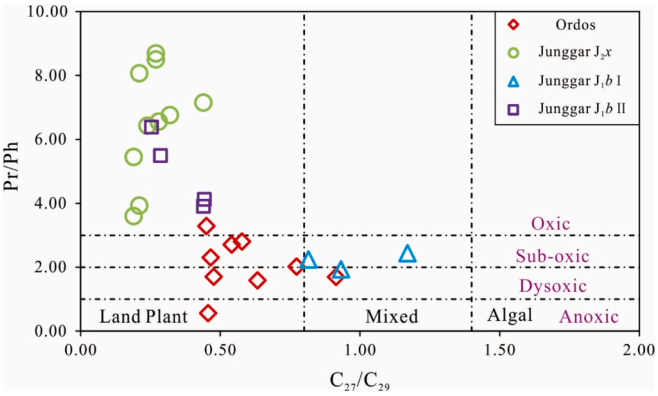

Fig. 8. Cross-plot of the C_{27}/C_{29} ααα-20R sterane ratio versus the pristane/phytane ratio for the coals from the Ordos and Junggar Basins (after Gorter, 2001).

Junggar basin, the $\delta^{13}C$ values of 4-MDBF and 2 + 3-MDBFs in J_2x (−25.9 ‰ to −25.8 ‰ and −26. 8 ‰ to −25.5 ‰) are much higher than those in J_1b (−31. 6 ‰ to −30.1 ‰, −29.5 ‰ to −29.4 ‰). However, the $\delta^{13}C$ values of DBF in J_2x (−26.2 ‰ to −25.4 ‰) are much lower than J_1b (−20.2 ‰ to −19.7 ‰) (Table 3).

5. Discussion

5.1. Palaeodepositional environments and organic matter source input

In this study, the depositional environments and origins of organic matter were attributed based on the distributions of biomarker indicators. The distributions of Pr and Ph are considered to be effective indicators of the redox conditions, even though they were influenced by many different geological factors (Didyk et al., 1978). In this study, the Pr/nC_{17} and Ph/nC_{18} ratios range from 0.29–11.65 and 0.08–1.69, respectively. The cross-plot of Pr/nC_{17} versus Ph/nC_{18} reveals that the Ordos basin samples were deposited under sub-oxic to oxic conditions; the J_2x and J_1b II samples were deposited under oxic conditions; and the J_1b I were deposited under sub-oxic to dysoxic conditions (Fig. 7).

The C_{27}/C_{29} sterane ratio can be used to determine the origins of organic matter (Nichols et al., 1990; Moore et al., 1992; Gorter, 2001). On the C_{27}/C_{29} steranes versus Pr/Ph cross-plot, most of the Ordos basin samples are located in the sub-oxic to dysoxic zones with terrestrial plant input. The J_2x and J_1b II samples are in the oxic zone with terrestrial plant input. However, the J_1b I samples fall within the sub-oxic-to-dysoxic zones with mixed terrestrial and algal input (Fig. 8). The Spearman's correlation between Pr/nC_{17} and R_o values ($|r| < 0.5$) in each three types of samples (Ordos, J_2x and J_1b) indicate that the effect of thermal maturity on Pr/nC_{17} is limited, but it has a relatively stronger impact on C_{27}/C_{29} ($0.34 < |r| < 0.74$) (Fig. S1; Table S1).

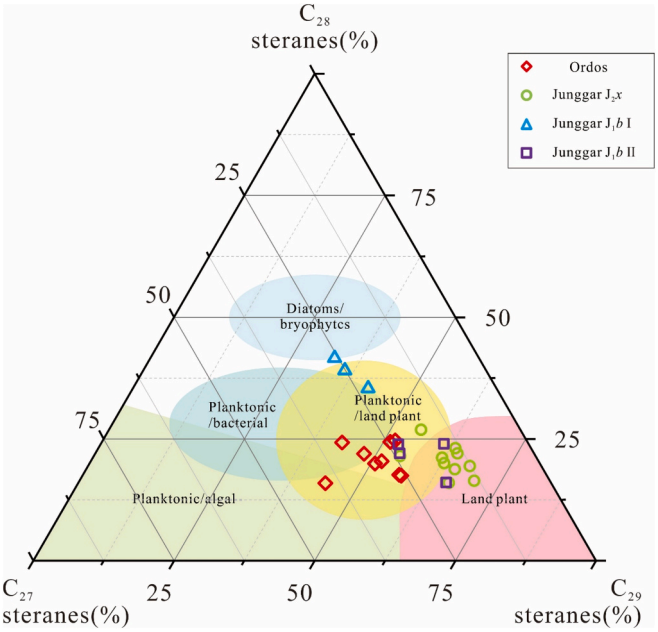

Fig. 9. Ternary diagram of regular steranes (C_{27}, C_{28}, and C_{29}) showing the relationship between sterane compositions and organic matter input (modified after Huang and Meinschein, 1979).

Moreover, sterane distributions are widely applied to predict OM source input. The ternary diagram of C_{27}-C_{28}-C_{29} ααα 20R steranes (Moldowan et al., 1985) shows mixed plankton and higher plant inputs for the Ordos basin samples. The J_2x and J_1b II samples fall mainly within the area of terrestrial plant input, and the J_1b I samples fall within the area of mixed plankton and land plant input, except a sample which in the area of plankton and bryophytes input (Fig. 9).

In summary, it is an acceptable conclusion that the OM in the Ordos basin samples was deposited in a transitional environment with sub-oxic to dysoxic conditions, dominated by mixed contributions of planktonic algae and terrigenous plants. The J_2x and J_1b II samples were sourced from terrigenous organic matter in oxic and terrestrial environments. In contrast, the OM in J_1b I samples was deposited in a transitional environment with algal and a bit bryophytes input under sub-oxic to dysoxic conditions.

5.2. Sources of PAH in the coal samples

Previous research has indicated that the relative abundances of PAHs can also be applied to determine their sources (Yunker et al., 2002; Budzinski et al., 1995; Gao et al., 2018; Zhao et al., 2023). In this study, the Fl/(Fl + Py), IPy/(IPy + BgP), 1,7-DMP/(1,7 + 2,6 + 3.,5-DMP), C_0/(C_0 + C_1) Fl/Py and BaA/(BaA + Chy) ratios were chosen as indicators of combustion/petrogenic sources (Yunker et al., 2002; Zakrzewski and Kosakowski, 2021). The cross plots of these ratios and R_o values with the results of Spearman's non-parametric correlation analysis of Ordos, J_2x and J_1b samples indicated that thermal maturity has limited influence on them (Table S1; Fig. S2).

Based on these indicators, the majority of samples appear to be predominantly of pyrolytic origin (Fig. 10). This is particularly true for J_2x and J_1b II, while Ordos and J_1b I suggest increased contributions from petrogenic sources (Table 2; Fig. 10). These results indicate that the occurrence of wildfires significantly affected the samples from J_2x, J_1b

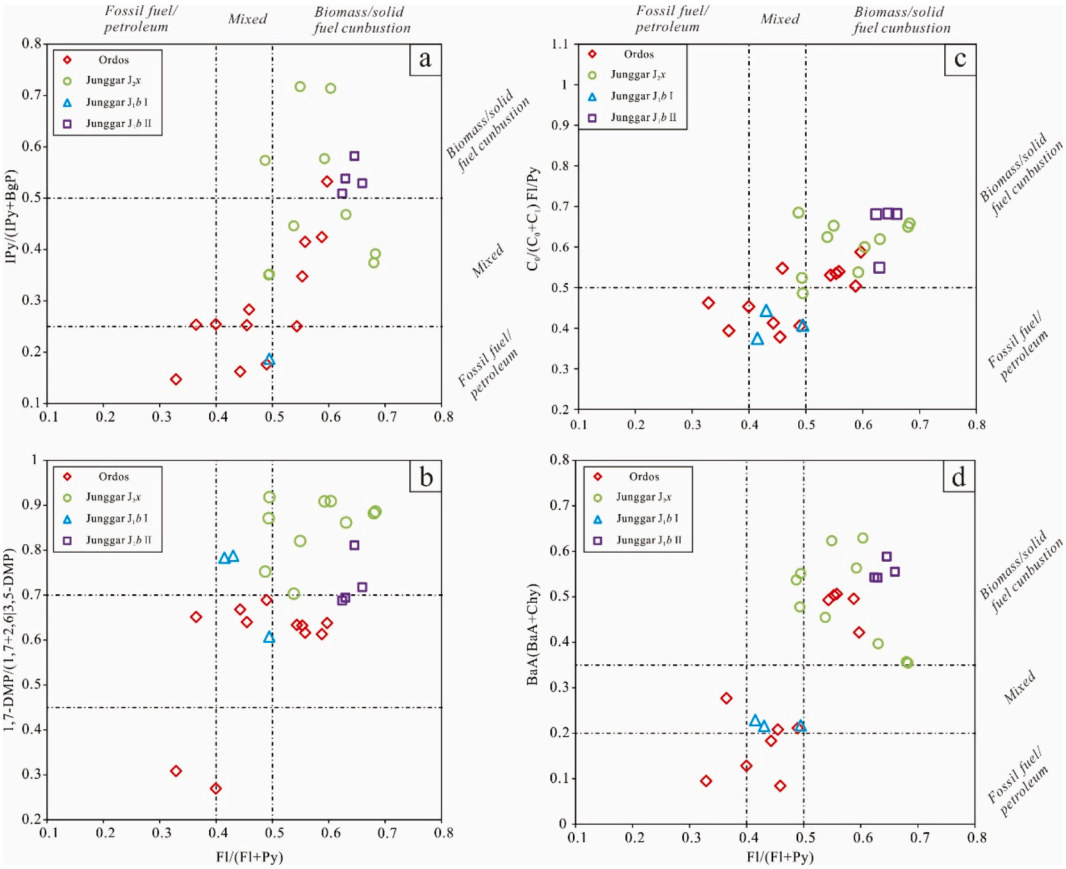

Fig. 10. Diagnostic plots indicating PAC origin. (a) Fl/(Fl + Py) vs IPy/(IPy + BgP) plot, (b) Fl/(Fl + Py) vs 1,7-DMP/(1,7 DMP + 2,6- + 3,5-DMP), (c) Fl/(Fl + Py) vs $C_0/(C_0 + C_1)$ Fl/Py and (d) Fl/(Fl + Py) vs BaA/(BaA + Chy). Fl: fluoranthene; Py: pyrene; DMP: dimethylphenantrene; BaA: benz[α]anthracene; Chy: chrysene.

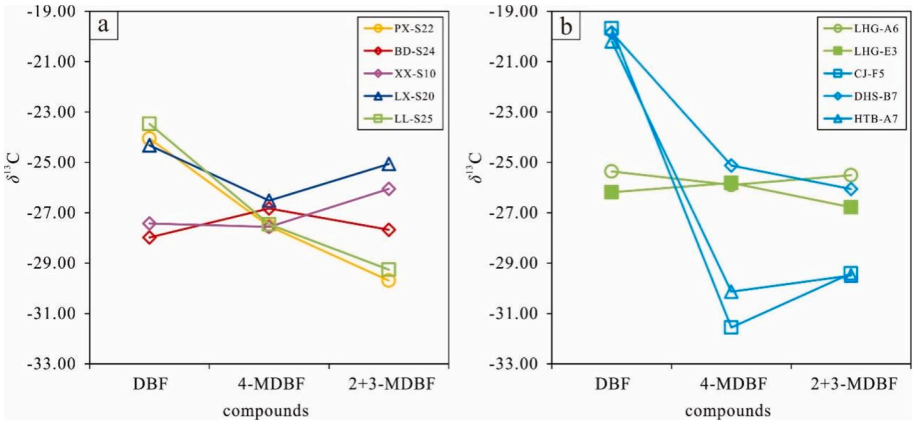

Fig. 11. $\delta^{13}C$ values of dibenzofuran and alkyldibenzofurans in selected coals. Fig. (a) is the $\delta^{13}C$ of DBF, 4-MDBF and 2 + 3-MDBFs in the Ordos basin samples. Fig. (b) is the $\delta^{13}C$ of the same compounds in the Junggar samples.

II, and parts of the Ordos basin but had a limited effect in other parts of the Ordos basin and in the J_1b I samples.

5.3. Factors reflected by the $\delta^{13}C$ values of dibenzofuran and methyldibenzofurans

5.3.1. The contributions of various plant types

The DBF homologous series may be products of incomplete combustion from either natural combustion sources or derived from biological precursors found in terrestrial plants and lichens (Sephton et al., 1999; Radke et al., 2000; Millot et al., 2016). DBF may derived from terrigenous higher plants, while MDBFs may have various sources, including lichens and higher plants (Liang et al., 2024). Previous research has indicated that the origin of organic matter is a crucial factor in determining the isotopic distribution of individual compounds (Galimov, 2006; Maslen et al., 2011; Cesar and Grice, 2017; Karp et al., 2020). It is supported that the OM from lichens, which are widely distributed in the environment similar to the coals in this study, are characterized by $\delta^{13}C$ ranges (~−30 ‰) lower than higher plants (≥−27 ‰) (Lakatos et al., 2007; Maslen et al., 2011).

These results also show up in $\delta^{13}C$ results of this study: the $\delta^{13}C$ values of DBF in all samples (average −25.5 ‰ in Ordos samples, −25.8

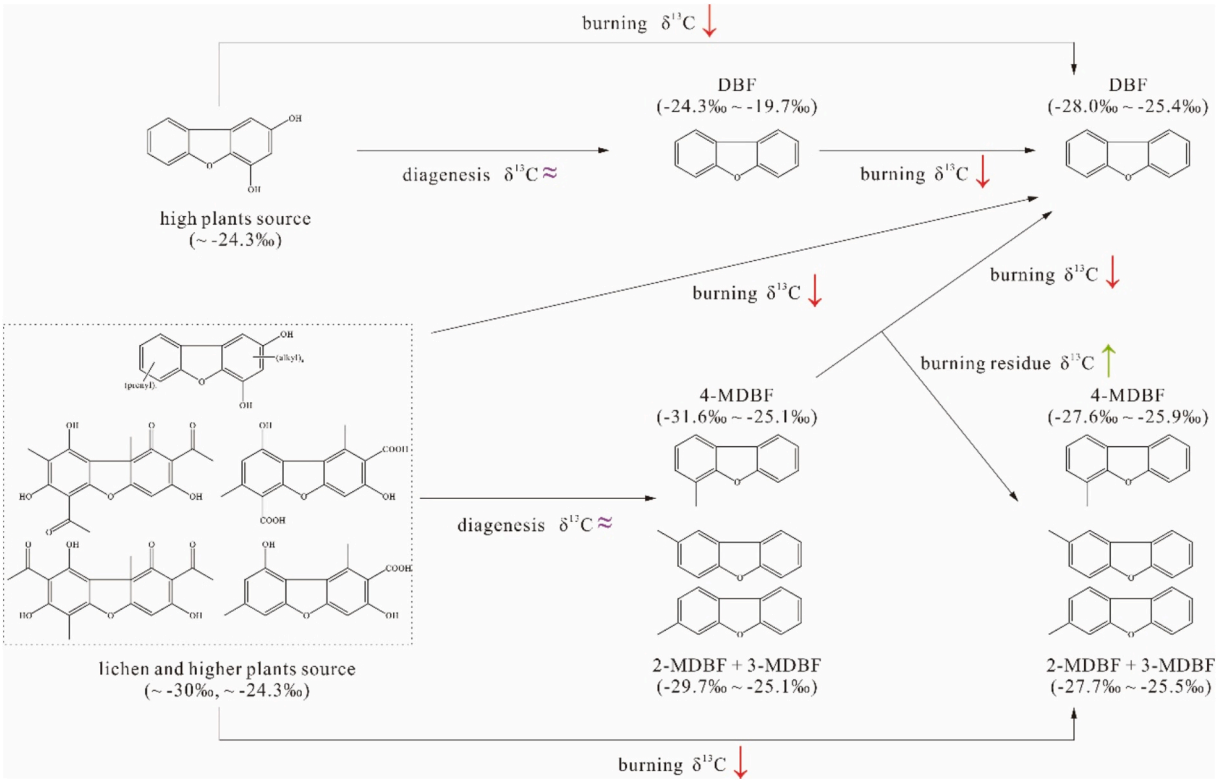

Fig. 12. Postulated structural transition and isotopic fractionation mechanism of MDBFs and DBF.

‰ in J_2x, and −19.9 ‰ in J_1b I samples) are higher than those of 4-MDBF (−27.2 ‰, −25.9 ‰, and −28.9 ‰) and 2 + 3-MDBF (−27.5 ‰, −26.1 ‰, and −28.3 ‰), especially in J_1b I samples (Table 3; Fig. 11). Our data suggests that the simple DBF compounds were isolated mainly from higher plants, and compounds with methyldibenzofurans structures (such as 4- and 2 + 3-DBFs) may derive from various sources, both lichens and higher plants.

5.3.2. *Minimal fractionation during the wildfire effects*

The DBF in the J_2x samples (−26.2 ‰ to −25.4 ‰) shows lower $\delta^{13}C$ values than in the J_1b samples (−20.2 ‰ to −19.7 ‰) (Table 3; Fig. 11). The J_1b samples, which are considered to have mixed origins of organic matter with more plankton input and show almost no influence from wildfires compared to the J_2x samples, have relatively higher $\delta^{13}C$ values of DBF. Conversely, the J_2x samples show lower $\delta^{13}C$ values of DBF, which coincides with the evidence of wildfires supported by the PAH indices and greater input from terrestrial plants (Fig. 8; Fig. 9; Fig. 10). This trend is also found in the Ordos Basin coals, especially in BD-S24 and XX-S10 (Table 3; Fig. 11a), although it is not as obvious as in J_2x samples. These trends may result from the lower input of land plants and mixed PAHs, which are eindicated by the biomarkers and PAH indices (Fig. 8; Fig. 9; Fig. 10), indicating that the impact of the wildfire was relatively less severe than on J_2x coals.

Transitions between compounds can also occur during combustion. Theoretical calculations using density functional theory and molecular dynamics simulations reveal that the reaction temperatures for methyl shift isomerization and the demethylation of these compounds are above 830.90 °C (Yang et al., 2019; Wang et al., 2020) —temperatures that can be exceeded during wildfire events. These records suggest that the fractionation process described above is possible (Fig. 12). Because of the activation energy for C–C bonds that include a ^{12}C methyl moiety, is lower than that of C–C bonds that include a ^{13}C methyl moiety (Galimov, 2006; Le Métayer et al., 2014). Our data suggest that preferential demethylation of ^{13}C-depleted MDBFs leads to ^{13}C enrichment of residual isomers. Increased wildfire activity in the J_2x samples resulted in DBFs with a higher contribution from combustion products, leading to lower $\delta^{13}C$ values than those in the J_1b coals, producing $\delta^{13}C$ values of MDBFs that are relatively higher and closer to that of DBF due to the increased input from higher plants (Table 3; Fig. 12). Furthermore, the ^{13}C-depleted products from these demethylation reactions contribute to lower $\delta^{13}C$ values of DBF in samples affected by wildfires (Fig. 12).

6. Conclusions

In this study, a molecular approach was complemented by a compound-specific isotope approach (CSIA) to differentiate the sources of individual PACs in coals from the Ordos and Junggar basins in western China. $\delta^{13}C$ values were obtained for various sub-classes of the aromatic fractions, such as DBF, 4-MDBF and 2 + 3-MDBF. In the case of coals, there is no systematic variation in the $\delta^{13}C$ values of individual PACs with increasing thermal maturation. The source of the OM is found to be a key factor in determining the isotopic distribution of PACs. The differences in $\delta^{13}C$ values between DBF and MDBFs are due to biogenic differences. DBF is derived from a single higher plant source, while MDBFs have multiple sources, including higher plants and various lichen species. The similarities between the $\delta^{13}C$ values for DBF and MDBFs in the heavily wildfire-affected samples are due to two factors: (1) The kinetic isotope effect led to enrichment of the residual MDBFs in the ^{13}C isotopes and enrichment of DBF in the ^{12}C isotopes. (2) A predominance of higher plant inputs over lichens resulted in higher $\delta^{13}C$ values for MDBFs.

CRediT authorship contribution statement

Ziao Geng: Writing – original draft. **Meijun Li:** Writing – review & editing. **Shuichang Zhang:** Investigation. **Shengbao Shi:** Software, Methodology. **Wenqiang Wang:** Investigation. **Lei Zhu:** Methodology, Resources. **Tiantian Li:** Software. **Jianfeng Zhang:** Software, Methodology.

Declaration of competing interest

The authors declare that they have no known competing financial interests or personal relationships that could have appeared to influence the work reported in this paper.

Acknowledgements

This work was funded by the National Natural Science Foundation of China (Grant No. 42202134). We would like to thank the National Key Laboratory of Petroleum Resource and Engineering, China University of Petroleum (Beijing) for providing samples and data, and for giving their permission to publish this work. The authors also wish to thank the Associate Editor and anonymous reviewers for their relevant comments that improved the quality of this manuscript.

Appendix A. Supplementary data

Supplementary data to this article can be found online at https://doi.org/10.1016/j.orggeochem.2025.105049.

Data availability

The authors do not have permission to share data.

References

Alexander, R., Bastow, T.P., Fisher, S.J., Kagi, R.I., 1995. Geosynthesis of organic compounds; II, methylation of phenanthrene and alkylphenanthrenes. Geochimica et Cosmochimica Acta 59, 4259–4266. https://doi.org/10.1016/0016-7037(95)00285-8.

Asif, M., Alexander, R., Fazeelat, T., Pierce, K., 2009. Geosynthesis of dibenzothiophene and alkyl dibenzothiophenes in crude oils and sediments by carbon catalysis. Organic Geochemistry 40, 895–901. https://doi.org/10.1016/j.orggeochem.2009.04.016.

Asif, M., Alexander, R., Fazeelat, T., Grice, K., 2010. Sedimentary processes for the geosynthesis of heterocyclic aromatic hydrocarbons and fluorenes by surface reactions. Organic Geochemistry 41, 522–530. https://doi.org/10.1016/j.orggeochem.2009.12.002.

Boreham, C.J., Summons, R.E., Roksandic, Z., Dowling, L.M., Hutton, A.C., 1994. Chemical, molecular and isotopic differentiation of organic facies in the Tertiary lacustrine Duaringa oil shale deposit, Queensland, Australia. Organic Geochemistry 21, 685–712. https://doi.org/10.1016/0146-6380(94)90013-2.

Budzinski, H., Garrigues, P., Connan, J., Devillers, J., Domine, D., Radke, M., Oudin, J.L., 1995. Alkylated phenanthrene distributions as maturity and origin indicators in crude oils and rock extracts. Geochimica et Cosmochimica Acta 59, 2043–2056. https://doi.org/10.1016/0016-7037(95)00125-5.

Cesar, J., Grice, K., 2017. $\delta^{13}C$ of polycyclic aromatic hydrocarbons to establish the facies variations in a fluvial deltaic Triassic record (Dampier sub-Basin, Western Australia). Organic Geochemistry 107, 59–68. https://doi.org/10.1016/j.orggeochem.2017.03.001.

Chen, Y., Tian, C., Li, K., Cui, X., Wu, Y., Xia, Y., 2016. Influence of thermal maturity on carbon isotopic composition of individual aromatic hydrocarbons during anhydrous closed-system pyrolysis. Fuel 186, 466–475. https://doi.org/10.1016/j.fuel.2016.08.102.

Dai, J.X., Li, J., Luo, X., Zhang, W.Z., Hu, G.Y., Ma, C.H., Guo, J.M., Ge, S.G., 2005. Stable carbon isotope compositions and source rock geochemistry of the giant gas accumulations in the Ordos Basin, China. Organic Geochemistry 36, 1617–1635. https://doi.org/10.1016/j.orggeochem.2005.08.017.

Didyk, B.M., Simoneit, B.R.T., Brassell, S.T., Eglinton, G., 1978. Organic geochemical indicators of palaeoenvironmental conditions of sedimentation. Nature 272, 216–222. https://doi.org/10.1038/272216a0.

Ellis, L., Singh, R.K., Alexander, R., Kagi, R.I., 1996. Formation of isohexyl alkylaromatic hydrocarbons from aromatization-rearrangement of terpenoids in the sedimentary environment: a new class of biomarker. Geochimica et Cosmochimica Acta 60, 4747–4763. https://doi.org/10.1016/S0016-7037(96)00281-5.

Galimov, E.M., 2006. Isotope organic geochemistry. Organic Geochemistry 37, 1200–1262. https://doi.org/10.1016/j.orggeochem.2006.04.009.

Gao, P., Li, H., Wilson, C.P., Townsend, T.G., Xiang, P., Liu, Y., Ma, L.Q., 2018. Source identification of PAHs in soils based on stable carbon isotopic signatures. Critical Reviews in Environmental Science and Technology 48, 923–948. https://doi.org/10.1080/10643389.2018.1495983.

Ge, T., Chang, X., Zhang, G., Zhang, J., Guo, R., Gao, W., Zhao, L., Wang, S., Duan, J., 2024. Understanding the hydrocarbon-generation potential on Jurassic coal-measure source rocks in the Junggar Basin: from the perspective of hydrogen-rich molecular structure. Petroleum Science 21, 2969–2983. https://doi.org/10.1016/j.petsci.2024.03.011.

Gorter, J., 2001. A marine source rock in the Gippsland Basin? In: Hill, K.H., Bernecker, T. (Eds.), Eastern Australasian Basins Symposium, a Refocussed Energy Perspective for the Future. Petroleum Exploration Society of Australia, Perspective for the Future, Melbourne, Special Publication, pp. 385–390. https://archives.datapages.com/data/petroleum-exploration-society-of-australia/conferences/001/001001/pdfs/385.html.

Han, Q., Liu, J., Shang, N., Zhao, S., Jia, R., 2024. Mineralogy and geochemistry of the Middle Jurassic coal in the southern Ordos Basin, China: responses of element geochemical behavior to climatic changes. Palaeogeography, Palaeoclimatology, Palaeoecology 648, 112284. https://doi.org/10.1016/j.palaeo.2024.112284.

He, T., Lamont, B.B., 2018. Baptism by fire: the pivotal role of ancient conflagrations in evolution of the Earth's flora. National Science Review 5, 237–254. https://doi.org/10.1093/nsr/nwx041.

Hua, F., Shao, L., Wang, X., Jones, T.P., Zhang, T., Bond, D.P.G., Yan, Z., Hilton, J., 2024. The impact of frequent wildfires during the Permian–Triassic transition: floral change and terrestrial crisis in southwestern China. Palaeogeography, Palaeoclimatology, Palaeoecology 641, 112129. https://doi.org/10.1016/j.palaeo.2024.112129.

Huang, W.Y., Meinschein, W.G., 1979. Sterols as ecological indicators. Geochimica et Cosmochimica Acta 43, 739–745. https://doi.org/10.1016/0016-7037(79)90257-6.

Hughes, W.B., Holba, A.G., Dzou, L.I., 1995. The ratios of dibenzothiophene to phenanthrene and pristane to phytane as indicators of depositional environment and lithology of petroleum source rocks. Geochimica et Cosmochimica Acta 59, 3581–3598. https://doi.org/10.1016/0016-7037(95)00225-O.

Jiang, L., George, S.C., 2019. Biomarker signatures of Upper Cretaceous Latrobe Group petroleum source rocks, Gippsland Basin, Australia: distribution and geological significance of aromatic hydrocarbons. Organic Geochemistry 138, 103905. https://doi.org/10.1016/j.orggeochem.2019.103905.

Jiang, L., George, S.C., 2020. Geochemical evaluation of aliphatic and aromatic hydrocarbons in Palaeogene source rocks from the Latrobe Group, Gippsland Basin, Australia. Marine and Petroleum Geology 120, 104516. https://doi.org/10.1016/j.marpetgeo.2020.104516.

Kappenberg, A., Braun, M., Amelung, W., Lehndorff, E., 2019. Fire condensates and charcoals: chemical composition and fuel source identification. Organic Geochemistry 130, 43–50. https://doi.org/10.1016/j.orggeochem.2019.01.009.

Karp, A.T., Holman, A.I., Hopper, P., Grice, K., Freeman, K.H., 2020. Fire distinguishers: refined interpretations of polycyclic aromatic hydrocarbons for paleo-applications. Geochimica et Cosmochimica Acta 289, 93–113. https://doi.org/10.1016/j.gca.2020.08.024.

Kilby, W.E., 1988. Recognition of vitrinite with non-uniaxial negative reflectance characteristics. International Journal of Coal Geology 9, 267–285. https://doi.org/10.1016/0166-5162(88)90017-1.

Konan, N.G.F.D., Li, M., Shi, S., Kojo, A., Toyin, A., Boakye, N.P.O., Li, T., 2022. Stable carbon isotopic composition of selected alkylnaphthalenes and alkylphenanthrenes from the Tarim oilfields, NW China. Energies 15, 7145. https://doi.org/10.3390/en15197145.

Lakatos, M., Hartard, B., Máguas, C., 2007. The stable isotopes $\delta^{13}C$ and $\delta^{18}O$ of lichens can be used as tracers of microenvironmental carbon and water sources. Terrestrial Ecology 1, 77–92. https://doi.org/10.1016/S1936-7961(07)01006-8.

Le Métayer, P., Grice, K., Chow, C.N., Caccetta, L., Maslen, E., Dawson, D., Fusetti, L., 2014. The effect of origin and genetic processes of low molecular weight aromatic hydrocarbons in petroleum on their stable carbon isotopic compositions. Organic Geochemistry 72, 23–33. https://doi.org/10.1016/j.orggeochem.2014.04.008.

Lei, Y., Cao, H., Wang, X., Zhang, D., Wang, W., Guo, X., 2022. Polycyclic aromatic hydrocarbons in the Upper Cretaceous lacustrine deposits from the Songliao Basin (NE China): implications for wildfires and paleoclimate. Palaeogeography, Palaeoclimatology, Palaeoecology 600, 111083. https://doi.org/10.1016/j.palaeo.2022.111083.

Li, J., Zhuang, X.G., Querol, X., Font, O., Moreno, N., Zhou, J.B., 2012. Environmental geochemistry of the feed coals and their combustion by-products from two coal-fired power plants in Xinjiang Province, Northwest China. Fuel 95, 446–456. https://doi.org/10.1016/j.fuel.2011.10.025.

Li, M., Simoneit, B.R.T., Zhong, N., Fang, R., 2013a. The distribution and origin of dimethyldibenzothiophenes in sediment extracts from the Liaohe Basin, East China. Organic Geochemistry 65, 63–73. https://doi.org/10.1016/j.orggeochem.2013.10.007.

Li, M., Wang, T., Zhong, N., Zhang, W., Sadik, A., Li, H., 2013b. Ternary diagram of fluorenes, dibenzothiophenes and dibenzofurans: indicating depositional environment of crude oil source rocks. Energy Exploration & Exploitation 31, 569–588. https://doi.org/10.1260/0144-5987.31.4.56.

Li, Y., Shao, L., Hou, H., Tang, Y., Yuan, Y., Zhang, J., Shang, X., Lu, J., 2018. Sequence stratigraphy, palaeogeography, and coal accumulation of the fluvio-lacustrine Middle Jurassic Xishanyao Formation in central segment of southern Junggar Basin, NW China. International Journal of Coal Geology 192, 14–38. https://doi.org/10.1016/j.coal.2018.04.003.

Li, Z., Huang, H., George, S.C., 2022. Unusual occurrence of alkylnaphthalene isomers in upper Eocene to Oligocene sediments from the western margin of Tasmania, Australia. Organic Geochemistry 168, 104418. https://doi.org/10.1016/j.orggeochem.2022.104418.

Liang, X., Chen, W., Jiang, B., Xiao, C., 2024. Dibenzofurans from nature: biosynthesis, structural diversity, sources, and bioactivities. Bioorganic Chemistry 144, 107107. https://doi.org/10.1016/j.bioorg.2024.107107.

Martins, L.L., Schulz, H.-M., Severiano Ribeiro, H.J.P., do Nascimento, C.A., de Souza, E. S., da Cruz, G.F., 2020. Cadalenes and norcadalenes in organic-rich shales of the Permian Irati Formation (Paraná Basin, Brazil): tracers for terrestrial input or also

indicators of temperature-controlled organic-inorganic interactions? Organic Geochemistry 140, 103962. https://doi.org/10.1016/j.orggeochem.2019.103962.
Marynowski, L., Kurkiewicz, S., Rakociński, M., Simoneit, B.R.T., 2011. Effects of weathering on organic matter: I. Changes in molecular composition of extractable organic compounds caused by paleoweathering of a lower Carboniferous (Tournaisian) marine black shale. Chemical Geology 285, 144–156. https://doi.org/10.1016/j.chemgeo.2011.04.001.
Maslen, E., Grice, K., Métayer, P.L., Dawson, D., Edwards, D., 2011. Stable carbon isotopic compositions of individual aromatic hydrocarbons as source and age indicators in oils from western Australian basins. Organic Geochemistry 42, 387–398. https://doi.org/10.1016/j.orggeochem.2011.02.005.
Mazeas, L., Budzinski, H., Raymond, N., 2002. Absence of stable carbon isotope fractionation of saturated and polycyclic aromatic hydrocarbons during aerobic bacterial biodegradation. Organic Geochemistry 33, 1259–1272. https://doi.org/10.1016/S0146-6380(02)00136-5.
Millot, M., Dieu, A., Tomasi, S., 2016. Dibenzofurans and derivatives from lichens and ascomycetes. Natural Product Reports 33, 801–811. https://doi.org/10.1039/C5NP00134J.
Moldowan, J.M., Seifert, W.K., Gallegos, E.J., 1985. Relationship between petroleum composition and depositional environment of petroleum source rocks. AAPG Bulletin 69, 1255–1268. https://doi.org/10.1306/AD462BC8-16F7-11D7-8645000102C1865D.
Moore, P.S., Burns, B.J., Emmett, J.K., Guthrie, D.A., 1992. Integrated source, maturation and migration analysis, Gippsland Basin, Australia. The APPEA Journal 32, 313–324. https://doi.org/10.1071/AJ91025.
Murray, A.P., Edwards, D., Hope, J.M., Boreham, C.J., Booth, W.E., Alexander, R.A., Summons, R.E., Horsfield, B., Radke, M., Schaefer, R.G., Wilkes, H., 1998. Carbon isotope biogeochemistry of plant resins and derived hydrocarbons. Organic Geochemistry 29, 1199–1214. https://doi.org/10.1016/S0146-6380(98)00126-0.
Nichols, P.D., Palmisano, A.C., Rayner, M.S., Smith, G.A., White, D.C., 1990. Occurrence of novel C_{30} sterols in Antarctic sea-ice diatom communities during a spring bloom. Organic Geochemistry 15, 503–508. https://doi.org/10.1016/0146-6380(90)90096-I.
Niu, C., Hou, D., Cheng, X., Han, X., 2023. Carbon isotopic compositions of mono-, di-, tri-aromatics provide insights into the source of sulfur-rich crude oils in the Huanghekou Depression, Bohai Bay Basin. Petroleum Science 20, 753–768. https://doi.org/10.1016/j.petsci.2022.09.012.
Niu, X., Fan, L., Yan, X., Zhou, G., Zhang, H., Jing, X., Zhang, M., 2024. Enrichment conditions and resource potential of coal-rock gas in Ordos Basin, NW China. Petroleum Exploration and Development 51, 1122–1137. https://doi.org/10.1016/S1876-3804(25)60530-1.
Peters, K., Walters, C.C., Molodowan, J., 2005. The Biomarker Guide. Biomarkers and Isotopes in the Environment and Human History. Cambridge University Press, Cambridge. https://doi.org/10.1017/CBO9780511524868.
Qin, X.L., Li, R.X., Xi, S.L., Yang, T., Cheng, J.H., Zhao, B.S., Wang, N., 2017. Hydrothermal alteration and its influence on quality of the Upper Palaeozoic gas reservoirs in eastern Ordos Basin (in Chinese with English abstract). Natural Gas Geoscience 28, 43–51. http://www.nggs.ac.cn/EN/10.11764/j.issn.1672-1926.2016.11.019.
Qian, Y., Zhang, T., Wang, Z.D., Tuo, J.C., Zhang, M.F., Wu, C.J., Tian, C.T., 2018. Organic geochemical characteristics and generating potential of source rocks from the Lower-Middle Jurassic coal-bearing strata in the East Junggar Basin, NW China. Marine and Petroleum Geology 93, 113–126. https://doi.org/10.1016/j.marpetgeo.2018.02.036.
Qi, Y., Ju, Y., Tan, J., Bowen, L., Cai, C., Yu, K., Zhu, H., Huang, C., Zhang, W., 2020. Organic matter provenance and depositional environment of marine-to-continental mudstones and coals in eastern Ordos Basin, China—evidence from molecular geochemistry and petrology. International Journal of Coal Geology 217, 103345. https://doi.org/10.1016/j.coal.2019.103345.
Radke, M., Welte, D.H., Willsch, H., 1982. Geochemical study on a well in the western Canada Basin; relation of the aromatic distribution pattern to maturity of organic matter. Geochimica et Cosmochimica Acta 46, 1–10. https://doi.org/10.1016/0016-7037(82)90285-X.
Radke, M., Welte, D.H., Willsch, H., 1986. Maturity parameters based on aromatic hydrocarbons: influence of the organic matter type. Organic Geochemistry 10, 51–63. https://doi.org/10.1016/0146-6380(86)90008-2.
Radke, M., Hilkert, A., Rullkötter, J., 1998. Molecular stable carbon isotope compositions of alkylphenanthrenes in coals and marine shales related to source and maturity. Organic Geochemistry 28, 785–795. https://doi.org/10.1016/S0146-6380(98)00048-5.
Radke, M., Vriend, S.P., Ramanampisoa, L.R., 2000. Alkyldibenzofurans in terrestrial rocks; Influence of organic facies and maturation. Geochimica et Cosmochimica Acta 64, 275–286. https://doi.org/10.1016/S0016-7037(99)00287-2.
Santamaria-Orozco, D., Horsfield, B., Di Primio, R., Welte, D.H., 1998. Influence of maturity on distributions of benzo-and dibenzothiophenes in Tithonian source rocks and crude oils, Sonda de Campeche, Mexico. Organic Geochemistry 28, 423–439. https://doi.org/10.1016/S0146-6380(98)00009-6.
Sephton, M.A., Looy, C.V., Veefkind, R.J., Visscher, H., Brinkhuis, H., de Leeuw, J.W., 1999. Cyclic diaryl ethers in a Late Permian sediment. Organic Geochemistry 30, 267–273. https://doi.org/10.1016/S0146-6380(99)00002-9.
Sephton, M.A., Pillinger, C.T., Gilmour, I., 2000. Aromatic moieties in meteoritic macromolecular materials: analyses by hydrous pyrolysis and $\delta^{13}C$ of individual compounds. Geochimica et Cosmochimica Acta 64, 321–328. https://doi.org/10.1016/j.gca.2012.12.042.
Shanmugam, G., 1985. Significance of coniferous rain forests and related organic matter in generating commercial quantities of oil, Gippsland Basin, Australia. AAPG Bulletin 69, 1241–1254. https://doi.org/10.1306/AD462BC3-16F7-11D7-8645000102C1865D.
Tang, S., Liu, S., Tang, D., Tao, S., Zhang, A., Pu, Y., Zhang, T., 2021. Occurrence of fluids in high dip angled coal measures: geological and geochemical assessments for southern Junggar Basin, China. Journal of Natural Gas Science and Engineering 88, 103827. https://doi.org/10.1016/j.jngse.2021.103827.
van Aarssen, B.G.K., Hessells, J.K.C., Abbink, O.A., de Leeuw, J.W., 1992. The occurrence of polycyclic sesqui-, tri-, and oligoterpenoids derived from a resinous polymeric cadinene in crude oils from Southeast Asia. Geochimica et Cosmochimica Acta 56, 1231–1246. https://doi.org/10.1016/0016-7037(92)90059-R.
van Aarssen, B.G.K., Bastow, T.P., Alexander, R., Kagi, R.I., 1999. Distributions of methylated naphthalenes in crude oils: indicators of maturity, biodegradation and mixing. Organic Geochemistry 30, 1213–1227. https://doi.org/10.1016/S0146-6380(99)00097-2.
van Aarssen, B.G.K., Alexander, R., Kagi, R.I., 2000. Higher plant biomarkers reflect palaeovegetation changes during Jurassic times. Geochimica et Cosmochimica Acta 64, 1417–1424. https://doi.org/10.1016/S0016-7037(99)00432-9.
Volkman, J.K., 2005. Sterols and other triterpenoids: source specificity and evolution of biosynthetic pathways. Organic Geochemistry 36, 139–159. https://doi.org/10.1016/j.orggeochem.2004.06.013.
Watson, J.S., Sephton, M.A., Looy, C.V., Gilmour, I., 2005. Oxygen-containing aromatic compounds in a late Permian sediment. Organic Geochemistry 36, 371–384. https://doi.org/10.1016/j.orggeochem.2004.10.006.
Wang, N., Li, M., Liu, X., Hong, H., Tian, X., Yang, C., Shi, S., Liu, P., 2020. Geochromatographic fractionation effect of methyldibenzofuran in dolomite reservoirs and its application in tracing oil filling pathways in the Sichuan Basin. Marine and Petroleum Geology 113, 104126. https://doi.org/10.1016/j.marpetgeo.2019.104126.
Widodo, S., Bechtel, A., Anggayana, K., Püttmann, W., 2009. Reconstruction of floral changes during deposition of the Miocene Embalut coal from Kutai Basin, Mahakam Delta, East Kalimantan, Indonesia by use of aromatic hydrocarbon composition and stable carbon isotope ratios of organic matter. Organic Geochemistry 40, 206–218. https://doi.org/10.1016/j.orggeochem.2008.10.008.
Wu, C., Zhang, M., Xiong, D., Tuo, J., Ma, W., Qian, Y., 2020. Gas generation from Jurassic coal measures at low mature stage and potential gas accumulation in the eastern Junggar Basin, China. Journal of Natural Gas Science and Engineering 84, 103692. https://doi.org/10.1016/j.jngse.2020.103692.
Xie, W., Tan, J., Wang, W., Jia, J., Liu, Z., Wu, J., Wang, Y., Song, X., 2022. Record of Middle Jurassic wildfire and its incidental mercury emissions in northern Qaidam Basin, China: evidence from the inertinite and mercury anomalies in coal. International Journal of Coal Geology 261, 104078. https://doi.org/10.1016/j.coal.2022.104078.
Yang, Y., Li, W., Ma, L., 2005. Tectonic and stratigraphic controls of hydrocarbon systems in the Ordos Basin: a multicycle cratonic basin in central China. AAPG Bulletin 89, 255–269. https://doi.org/10.1306/10070404027.
Yang, S., Li, M., Liu, X., Han, Q., Wu, J., Zhong, N., 2019. Thermodynamic stability of methyldibenzothiophenes in sedimentary rock extracts: based on molecular simulation and geochemical data. Organic Geochemistry 129, 24–41. https://doi.org/10.1016/j.orggeochem.2018.10.012.
Yunker, M.B., Macdonald, R.W., Vingarzan, R., Mitchell, R.H., Goyette, D., Sylvestre, S., 2002. PAHs in the Fraser River basin; a critical appraisal of PAH ratios as indicators of PAH source and composition. Organic Geochemistry 33, 489–515. https://doi.org/10.1016/S0146-6380(02)00002-5.
Zakrzewski, A., Kosakowski, P., 2021. Impact of palaeo-wildfires on higher plant parameter revealed by new biomarker indicator. Palaeogeography, Palaeoclimatology, Palaeoecology 579, 110606. https://doi.org/10.1016/j.palaeo.2021.110606.
Zhao, C., Zhang, K., Xiao, L., Uhl, D., Shi, Z., Zhao, W., Zhao, Q., Sun, Y., Liu, B., 2023. Paleoclimate-induced wildfires in a paleomire in the Ordos Basin, northern China during the Middle Jurassic greenhouse period. Chemical Geology 637, 121677. https://doi.org/10.1016/j.chemgeo.2023.121677.
Zhu, Z., Li, M., Tang, Y., Qi, L., Leng, J., Liu, X., Xiao, H., 2019. Identification of phenyldibenzothiophenes in coals and the effects of thermal maturity on their distributions based on geochemical data and theoretical calculations. Organic Geochemistry 138, 103910. https://doi.org/10.1016/j.orggeochem.2019.103910.
Zhu, Z., Li, M., Li, J., Qi, L., Liu, X., Xiao, H., Leng, J., 2022. Identification, distribution and geochemical significance of dinaphthofurans in coals. Organic Geochemistry 166, 104399. https://doi.org/10.1016/j.orggeochem.2022.104399.